arXiv:1304.4143v1 [quant-ph] 15 Apr 2013

Chemical compass for avian magnetoreception as a quantum coherent device

Jianming Cai[1, 2] and Martin B. Plenio[1, 2]
[1] *Institut für Theoretische Physik, Albert-Einstein Allee 11, Universität Ulm, 89069 Ulm, Germany*
[2] *Center for Integrated Quantum Science and Technology, Universität Ulm, 89069 Ulm, Germany*

(Dated: April 16, 2013)

It is known that more than 50 species use the Earth's magnetic field for orientation and navigation. Intensive studies particularly behavior experiments with birds provide support for a chemical compass based on magnetically sensitive free radical reactions as a source of this sense. However, the fundamental question of whether and how quantum coherence plays an essential role in such a chemical compass model of avian magnetoreception yet remains controversial. Here, we show that the essence of the chemical compass model can be understood in analogy to a quantum interferometer exploiting quantum coherence. Within the framework of quantum metrology, we quantify quantum coherence and demonstrate that it is a resource for chemical magnetoreception. Our results allow us to understand and predict how various factors can affect the performance of a chemical compass from the unique perspective of quantum coherence assisted metrology. This represents a crucial step to affirm avian magnetoreception as an example of quantum biology, which exhibits a direct connection between quantum coherence and biological function.

Despite the growing interest from chemists and biologist and more recently researchers from quantum physics and quantum information, there remain to date only a handful of biological phenomena that are suspected or proven to rely on quantum effects. These include important biological processes such as light harvesting [1–6], the human sense of smell [7–9] and avian magnetoreception [10–15, 17–25]. The effects of weak magnetic field in nature have been observed for a long time [26], ranging from the growth of plants to the remarkable orientation and navigation abilities of birds, mammals, reptiles, amphibians, fish, crustaceans and insects. There are two principal mechanisms that may account for avian magnetoreception: one based on magnetically sensitive free radical reactions [10–16] and the other on magnetic iron minerals [27]. The radical pair mechanism, which was put forward to explain a variety of magnetic effects on free radical reactions [28] in spin chemistry experiments [29], suggests that the avian compass relies on magnetically sensitive radical pairs formed by photoinduced electron transfer reactions [10–15]. The cryptochromes in the retina of migratory birds provides a potential physiological implementation of such a mechanism [11, 30–38]. The numerous behavior experiments with birds [40], such as European robins, have shown that the magnetic orientation of birds responds to the inclination of the Earth's magnetic field, and is dependent on the wavelength of the ambient light [39]. Together with the finding that the navigation can be disrupted by very weak external oscillating magnetic fields [41], these observations provide corroborating evidence for the idea that the chemical compass mechanism is involved in avian magnetoreception.

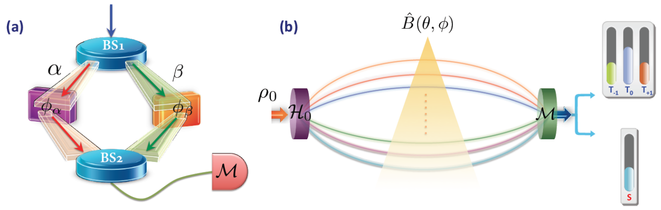

FIG. 1: **Quantum interferometer model of chemical compass.** **(a)** A quantum system, e.g. a photon or a spin, is prepared (BS_1) in a coherent superposition of two quantum states $|\alpha\rangle$ and $|\beta\rangle$, which undergoes different evolution paths dependent on an unknown physical parameter. The measurement after the interference (BS_2) of two paths reveals the information on the unknown parameter. **(b)** A chemical compass is viewed as a quantum interferometer, the hyperfine coupling Hamiltonian $\mathcal{H}_0$ recasts the state ρ_0 of the combined system of radical pair and nuclei into a superposition of its eigenstates. The weak magnetic field induces the change of coherence phases between different eigenstate evolution paths. The spin-dependent chemical reaction channels lead to the observable that reveal the interference of coherence phases.

In the last few years, the interest in the long-standing problem of avian magnetoreception has quickly extended from chemists and biologists to quantum physicists [17–25]. Although the detailed biophysical mechanisms underlying the chemical compass model of avian magnetoreception are quite complex and their details remain poorly understood, the radical pair model essentially involves two unpaired electrons (i.e. a pair of radicals) created in spin singlet or triplet states [10, 11, 29]. The subsequent dynamics is composed of a quantum coherent interaction between the spins as well as an interaction with a nuclear spin environment. The former supports quantum coherence while the latter is usually considered as a noise process that suppresses quantum coherence. In previous consideration emphasis was placed on the electronic coherence properties and it remained unclear how this coherence was related to the function of the chemical compass.

In the present work, we demonstrate that it is essential to go beyond this picture and to consider the combined system of both radical pair electron spins and the surrounding nuclear spins as the core of chemical magnetoreception. This leads us to appreciate that the quantum dynamics giving rise to the magnetic sensitivity is akin to a quantum interferometer in quantum metrology [42–44]. Indeed, the global electron-nuclear spin coherence, with respect to the eigenbasis of the hyperfine Hamiltonian, is found to be essential for the function of a chemical compass. The validation of this viewpoint depends on an appropriate quantification of coherence (see supplementary information for more discussions). To this end we introduce a simple and operationally motivated measure of quantum coherence, and show its relation with the magnetic sensitivity of a chemical compass. In contrast to studies that are only accounting for electron spin coherence (which we will denote as local quantum coherence to differentiate it from the concept of global quantum coherence put forward here) [20–24], our approach will clearly illustrate the essential role of quantum coherence in chemical magnetoreception.

Quantum interferometer model of chemical compass.— In quantum metrology, a system, e.g. a photon or a spin, is initially prepared into the following state

$$\rho_0 = |\Psi_0\rangle\langle\Psi_0|, \quad \text{with} \quad |\Psi_0\rangle = \gamma_\alpha|\alpha\rangle + \gamma_\beta|\beta\rangle, \tag{1}$$

which is written in the basis of $\{|\alpha\rangle, |\beta\rangle\}$ (determined by the interferometric element BS1, see Fig.1). A Hamiltonian $H(\lambda) = \frac{\lambda}{2}\left(|\alpha\rangle\langle\alpha| - |\beta\rangle\langle\beta|\right)$ parametrized by a single unknown parameter λ results in an evolution that changes the relative phase between the two states $|\alpha\rangle$ and $|\beta\rangle$ to $\Phi_\lambda = \varphi_\alpha - \varphi_\beta$, see Fig.1(a), and leads to the state

$$\rho_0 \to \rho_{\Phi_\lambda} = \begin{pmatrix} |\gamma_\alpha|^2 & \gamma_\alpha\gamma_\beta^* e^{i\Phi_\lambda} \\ \gamma_\alpha^*\gamma_\beta e^{-i\Phi_\lambda} & |\gamma_\beta|^2 \end{pmatrix}. \tag{2}$$

The measurement of the observable $\mathcal{M} = |\Psi_0\rangle\langle\Psi_0|$, gives the interference (see BS2 in Fig.1) outcome as

$$m_\lambda(\rho_0, \Phi_\lambda) \equiv \mathrm{Tr}\left(\rho_{\Phi_\lambda}\mathcal{M}\right) = 1 - 2|\gamma_\alpha|^2|\gamma_\beta|^2\left(1 - \cos\Phi_\lambda\right). \tag{3}$$

The precision of parameter estimation with such a basic quantum interferometer is determined by the contrast of the interference fringe as follows

$$\mathrm{D}_{\vec{\gamma}}(\rho_0) \equiv \max_{\Phi_\lambda} m_\lambda(\rho_0, \Phi_\lambda) - \min_{\Phi_\lambda} m_\lambda(\rho_0, \Phi_\lambda) = 2|\gamma_\alpha|^2|\gamma_\beta|^2. \tag{4}$$

The role of coherence in such a simple interferometric setup can be quantified by

$$\mathcal{C} \equiv |m_\lambda(\rho_0^c, \Phi_\lambda)|_{\Phi_\lambda = 0} \propto |\gamma_\alpha|^2|\gamma_\beta|^2, \tag{5}$$

with

$$\rho_0^c = \frac{1}{2}\begin{pmatrix} 0 & \gamma_\alpha\gamma_\beta^* \\ \gamma_\alpha^*\gamma_\beta & 0 \end{pmatrix}, \tag{6}$$

which characterizes how coherent the quantum interferometer is. The above definition is operational as it connects coherence to metrological precision and is thus preferable over alternative abstract measures of coherence, e.g. the summation of the absolute values of the off-diagonal density matrix elements (see supplementary information for detailed discussions). One can see that in the above simple setting of quantum interferometer, coherence is an essential ingredient for quantum metrology. Such a framework now allows us to clearly identify the role of coherence in chemical magnetoreception exploiting the analogy between a quantum interferometer and a chemical compass (see supplementary information for a complete list of analogies).

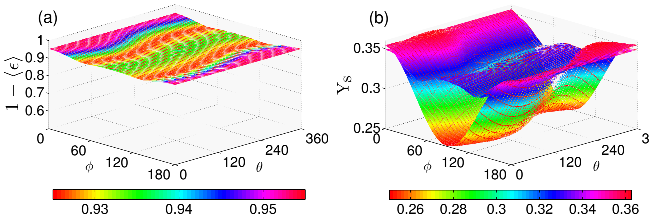

FIG. 2: **Effective evolution of a chemical compass under a weak magnetic field**. **(a)** The change of the absolute values of the (coherent) density elements $\langle\epsilon(t)\rangle$ averaging over time, with $\epsilon(t) = [\sum_{m\neq n}(r_{mn}^t - r_{mn})^2]^{1/2}$, for the flavin-superoxide radical pair with different magnetic field directions (θ, φ). **(b)** The singlet yield $\mathrm{Y_S}$ of the flavin-superoxide radical pair as the function of the magnetic field direction (θ, φ) including (lower) *vs.* excluding (upper) the coherence phase changes $\varphi_{mn}^{\hat{B}}(t)$ resulting from the weak magnetic field, see Eq.(10). The reaction rates are $k_S = k_T = 0.5\mu s^{-1}$, and the strength of the magnetic field is $b = 50\mu T$.

In the standard model of the chemical compass, the magnetically sensitive radical pairs formed by photo-induced intramolecular electron transfer reactions interact with a few nearby nuclei via hyperfine couplings, as described by the following Hamiltonian

$$\mathcal{H}_0 = \sum_{k=\mathcal{D},\mathcal{A}}\sum_j \vec{\mathbf{s}}_k \cdot \hat{\mathbf{T}}_{k_j} \cdot \vec{\mathbf{I}}_{k_j} \tag{7}$$

where $\vec{\mathbf{I}}_{k_j}$ and $\vec{\mathbf{s}}_k$ are the electron and nuclear spin operators respectively, $\hat{\mathbf{T}}_{k_j}$ denotes the hyperfine coupling tensors [29]. For simplicity, we neglect the dipole-dipole and exchange interactions between two radicals, which is valid when the radical-radical distance is sufficiently large or they cancel with each other [45]. The initial joint state ρ_0 of the radical pair and nuclear spins, written in the eigenbasis $\{|\nu_m\rangle\}$ of the hyperfine interaction Hamiltonian $\mathcal{H}_0$, can be expressed as

$$\rho_0 = \sum_{m,n} r_{mn}|\nu_m\rangle\langle\nu_n|, \quad \text{with} \quad r_{mn} = \langle\nu_m|\rho_0|\nu_n\rangle. \tag{8}$$

In the absence of a magnetic field, the state evolution solely under the hyperfine interaction Hamiltonian $\mathcal{H}_0$ is

$$\rho^{\mathcal{H}_0}(t) = \sum_{m,n} r_{mn} e^{-i\varphi^0_{mn}(t)} |\nu_m\rangle\langle\nu_n|. \tag{9}$$

For a typical radical pair molecule with a few nuclei [46], the leading order effect of the external magnetic field $\hat{\mathrm{B}} = -g\mu_b \vec{b}\cdot(\vec{\mathbf{s}}_{\mathcal{D}}+\vec{\mathbf{s}}_{\mathcal{A}})$ (with $|\vec{b}| = 50\mu\mathrm{T}$, which is much smaller than the typical interaction strength between the radical pair electron spin and the nearby nuclear spins) is to introduce an additional magnetic field dependent phase on the system coherence, namely

$$\rho^{\mathcal{H}_0+\hat{\mathrm{B}}(\theta,\varphi)}(t) \approx \sum_{m,n} r^t_{mn} e^{-i\left[\varphi^0_{mn}(t)+\varphi^{\hat{B}}_{mn}(t)\right]} |\nu_m\rangle\langle\nu_n|, \tag{10}$$

where $\rho^{\mathcal{H}_0+\hat{\mathrm{B}}(\theta,\varphi)}(t)$ represents the state evolution under the total Hamiltonian $\mathcal{H} = \mathcal{H}_0 + \hat{\mathrm{B}}(\theta,\varphi)$ including both the hyperfine coupling and the weak magnetic field. The effect of the external weak magnetic field might also change the absolute values of the coherent off-diagonal density matrix elements r_{mn} ($m \neq n$), which can be quantified by $\epsilon(t) = [\sum_{m\neq n}(r^t_{mn} - r_{mn})^2]^{1/2}$. In Fig.2, we plot ϵ averaging over time for the possible candidate radical pair flavin-superoxide in cryptochrome flavoprotein [14, 15] for different magnetic field directions (θ,φ), which shows that the change of the absolute values of the density matrix elements is very small and has a negligible effect on the magnetic sensitivity in the physiologically relevant regime (see supplementary information for more details).

The spin-dependent reactions in a chemical compass, i.e. the singlet and triplet radical pairs will undergo different chemical reaction paths and thereby lead to different chemical consequences [11], that witness the magnetic field effect on the radical pair dynamics by the magnetic anisotropy of reaction yield. For simplicity, we consider the scenarios where the reaction rates of the singlet and the triplet radicals are identical, i.e. $k_S = k_T \equiv k$ (see supplementary information for the generalization to more general cases). Treating the system dynamics with the conventional Haberkorn approach [29], the singlet yield can be formulated as

$$\mathrm{Y_S}(\mathcal{H}_0,\rho_0,\theta,\varphi) = \int \mathrm{Tr}\left[\rho^{\mathcal{H}_0+\hat{\mathrm{B}}(\theta,\varphi)}(t)\mathcal{M}\right] dt \tag{11}$$

with the observable $\mathcal{M} = ke^{-kt}(|\mathcal{S}\rangle\langle\mathcal{S}| \otimes_{k_j} \mathbb{I}_{d_{k_j}})$. The singlet yield in Eq.(11) can be viewed as a continuous generalization of the outcome in a quantum interferometer as $m_\lambda(\rho_0,\Phi_\lambda)$, see Eq.(2). With the example of flavin-superoxide radical pair, we show in Fig.2(b) that the magnetic anisotropy of singlet yield mainly comes from the coherent phase changes $\varphi^{\hat{B}}_{mn}(t)$ induced by the external weak magnetic field, as in the interference based quantum metrology.

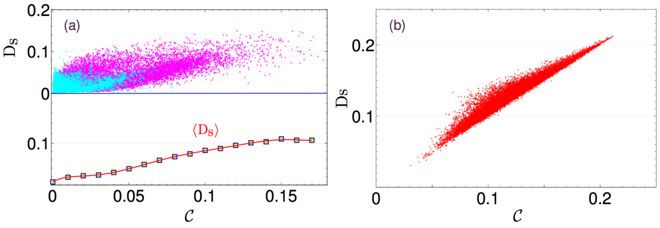

FIG. 3: **The relation between the coherence and the magnetic sensitivity of a chemical compass**. **(a)** The magnetic field sensitivity $\mathrm{D_S}(\mathcal{H}_0,\rho_0)$ as defined in Eq.(12) **(upper)** and the average value $\langle\mathrm{D_S}\rangle$ **(lower)** as a function of quantum coherence $\mathcal{C}(\mathcal{H}_0,\rho_0)$ given by Eq.(14) for 7×10^4 random hyperfine configurations of $5\sim6$ nuclei with the depolarized initial nuclear spin states. The violet dots represent these configurations of reference-and-probe type radical pair molecules, which has one radical free of hyperfine coupling. **(b)** The magnetic field sensitivity $\mathrm{D_S}(\mathcal{H}_{\mathrm{fo}},\rho_0)$ as a function of coherence measured by $\mathcal{C}(\mathcal{H}_{\mathrm{fo}},\rho_0)$ for the flavin-superoxide radical pair (whose hyperfine interaction Hamiltonian is denoted as $\mathcal{H}_{\mathrm{fo}}$) starting from 2×10^4 initial states, each has the singlet born radical pair and random nuclear spin polarizations. In both panels, the reaction rates are $k_S = k_T = 0.5\mu s^{-1}$, and the strength of the magnetic field is $b = 50\mu T$.

Quantum coherence and magnetic sensitivity.— Following the inspiration from quantum metrology, we continue to quantify the effect of quantum coherence in the present scenario of chemical magnetoreception. The function of a chemical compass starting from the state ρ_0 can be characterized by the magnetic anisotropy of the singlet yield defined as follows

$$\mathrm{D_S}(\mathcal{H}_0,\rho_0) = \max_{\theta,\varphi}\mathrm{Y_S}(\mathcal{H}_0,\rho_0,\theta,\varphi) - \min_{\theta,\varphi}\mathrm{Y_S}(\mathcal{H}_0,\rho_0,\theta,\varphi) \tag{12}$$

Henceforth we will call $\mathrm{D_S}(\mathcal{H}_0,\rho_0)$ as the magnetic sensitivity of a chemical compass. The coherent part of the system state ρ_0 is denoted as

$$\mathcal{GC}(\mathcal{H}_0,\rho_0) = \sum_{m\neq n} r_{mn}|\nu_m\rangle\langle\nu_n|. \tag{13}$$

To quantify the role of coherence in chemical magnetoreception, in the same spirit of quantifying the role of coherence in the interference based quantum metrology (see Eq.(5)), we introduce the following measure of global electron-nuclear quantum coherence for a chemical compass with a given hyperfine interaction Hamiltonian $\mathcal{H}_0$ and a system state ρ_0 as follows

$$\mathcal{C}(\mathcal{H}_0,\rho_0) = |\mathrm{Y_S}(\mathcal{H}_0,\mathcal{GC}(\mathcal{H}_0,\rho_0))|_{b=0} \tag{14}$$

which represents the contribution of coherence to the singlet yield in the absence of the external magnetic field.

To demonstrate the connection between coherence and the magnetic sensitivity in a chemical compass, we randomly sample a large number of hyperfine configurations and plot the relation between coherence $\mathcal{C}(\mathcal{H}_0,\rho_0)$

and the magnetic sensitivity $\mathrm{D}_{\mathcal{H}_0,\mathrm{S}}(\rho_0)$, where $\rho_0 = |\mathcal{S}\rangle\langle\mathcal{S}|\bigotimes_{k_j}(\mathbb{I}_{d_{k_j}}/d_{k_j})$, see Fig.3(a). The result shows that typically coherence is necessary for a high magnetic sensitivity of chemical magnetoreception. Furthermore, we also find that the reference-and-probe type of radical pairs (namely one radical of which is free from hyperfine coupling) [15, 16] which tends to result in the highest sensitivity usually embody larger coherence. This explains such an optimal design principle for a chemical compass from the perspective that coherence is a resource for chemical magnetoreception. Considering the specific example of the flavin-superoxide radical pair in cryptochrome protein, we plot in Fig.3(b) the magnetic sensitivity as a function of quantum coherence from a number of randomly chosen initial states of the singlet born radical pair but with different nuclear spin polarizations. The same feature is observed, namely the larger coherence the better magnetic sensitivity. We remark that the initial state in realistic radical pair reactions are usually given by the singlet or triplet radical pair state with depolarized nuclear spin states. We assume here a larger state space to facilitate the explicit demonstration of how coherence (that changes with the nuclear polarization) can directly affect the function of chemical magnetoreception. In experiments, this may be achieved by chemically induced dynamic nuclear polarization or with the assistance of well controllable quantum systems, e.g. nitrogen-vacancy centers in diamond [47–49]. In fact, both the magnetic field sensitivity and the coherence from a initial state with the depolarized nuclear spin state are almost identical to the average of these random samples with various nuclear polarizations. We also stress that the above measure of coherence in Eq.(14) is only determined by the hyperfine interaction Hamiltonian $\mathcal{H}_0$ (without an external magnetic field) and the initial state ρ_0, yet it well predicts the property (namely the magnetic sensitivity) of the dynamics of a chemical compass under a weak external magnetic field.

An unified picture of decoherence effects.— Following the present insight that quantum coherence of the global electron-nuclear state is a resource for chemical magnetoreception, it is possible to study the effects of different decoherence models on the functioning of a chemical compass [21–24] in a unified picture. More specifically, we can study how decoherence will destroy the global electron-nuclear quantum coherence in a chemical compass, as characterized by Eq.(14), and thereby deteriorate its magnetic anisotropy of reaction yield. Since a chemical compass shall work under ambient conditions, the noise from the environment of the core system (i.e. the radical pair and the surrounding nuclear spins) will inevitably affect its function. The noise effects varies for different decoherence models, which can be described by the following Lindblad type quantum master equation

$$\frac{\mathrm{d}}{\mathrm{dt}}\rho = -i[\mathcal{H},\rho] - \frac{k_S}{2}[Q_S,\rho]_+ - \frac{k_T}{2}[Q_T,\rho]_+ + \mathcal{L}(\rho) \quad (15)$$

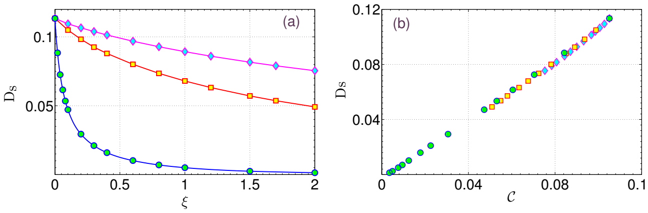

FIG. 4: **The noise effect of difference types of noise on the magnetic sensitivity of a chemical compass**. **(a)** The magnetic sensitivity $\mathrm{D_S}(\mathcal{H}_0,\rho_0)$ of the flavin-superoxide radical pair as a function of the decoherence rate ξ. **(b)** The magnetic sensitivity $\mathrm{D_S}(\mathcal{H}_0,\rho_0)$ as a function of the coherence $\mathcal{C}(\mathcal{H}_0,\rho_0)$ for the local dephasing (red, square), the electron spin relaxation (blue, circle), and the singlet-triplet dephasing (violet, diamond). The reaction rates are $k_S = k_T = 0.5\mu s^{-1}$, and the strength of the magnetic field is $b = 50\mu T$.

with

$$\mathcal{L}(\rho) = \sum_k \xi_k\left[\mathcal{L}_k\rho\mathcal{L}_k^\dagger - \frac{1}{2}\left(\mathcal{L}_k^\dagger\mathcal{L}_k\rho - \rho\mathcal{L}_k^\dagger\mathcal{L}_k\right)\right], \quad (16)$$

where $\mathcal{H} = \mathcal{H}_0 + \hat{\mathrm{B}}(\theta,\varphi)$ is the total Hamiltonian including the hyperfine interactions $\mathcal{H}_0$ and the external magnetic field $\hat{\mathrm{B}}(\theta,\varphi)$, Q_S and Q_T are the projectors into the singlet and triplet subspace of the radical pair state individually, and $[x,y]_+ = xy + yx$. The above master equation is based on the Haberkorn approach [29] by adding the dissipator $\mathcal{L}(\rho)$ which represent noises. We remark that it is not trace preserving as it is restricted in the subspace of active radical pair state, and the singlet yield can then be calculated as $\mathrm{Y_S} = k_S\int\langle\mathcal{S}|\rho(t)|\mathcal{S}\rangle dt$, which is equivalent to Eq.(11) in the absence of decoherence (see supplementary information and Ref.[18]). We consider three typical classes of noises, namely the local dephasing model $\mathcal{L}_I = \{\sigma_z^D, \sigma_z^A\}$ with $\sigma_z = |\alpha\rangle\langle\alpha| - |\beta\rangle\langle\beta|$, the spin relaxation $\mathcal{L}_{II} = \{\sigma_\pm^D, \sigma_\pm^A\}$ with $\sigma_+ = |\alpha\rangle\langle\beta|$ and $\sigma_- = |\beta\rangle\langle\alpha|$, and the singlet-triplet dephasing model [50] $\mathcal{L}_{III} = \{\sigma_{ST}^{DA}\}$ with $\sigma_{ST} = 2|\mathcal{S}\rangle\langle\mathcal{S}| - \mathbb{I}$, where the superscript D and A represent the two radicals. These decoherence models are all relevant in the radical pair mechanism but behave very different from each other in the sense that they destroy varying aspects of local electron spin coherence of radical pairs: they will respectively lead to the decay of local electron spin coherence, of electron spin longitudinal component, and of singlet-triplet coherence at a rate given by $\xi_k \equiv \xi$.

In Fig.4(a), one can see that the effects of these noise models on the magnetic sensitivity of the flavin-superoxide radical pair are quantitatively very different as a function of the same decoherence rate ξ. Such a fact is natural but gives no general insight into the problem how and why different types of noise would affect chemical magnetoreception to different extent. Instead, we use the proposed measure of coherence $\mathcal{C}(\mathcal{H}_0,\rho_0)$ and find a universal relation between the decoherence effects on the magnetic sensitivity and the coherence, which holds for different noise models studied here, see Fig.4(b). This supports the observation that the global electron-nuclear coherence is indeed responsible for the magnetic sensitivity of a chemical compass. Furthermore, by studying the effect of noise on the coherence one can predict its effect on the magnetic field sensitivity on the basis of its direct connection to the global electron-nuclear coherence.

Discussions.— We have introduced the viewpoint of chemical magnetoreception as a quantum interferometer. This perspective allows us to reveal that quantum coherence in the joint basis of the hyperfine interaction Hamiltonian of the radical pair electron spins *and* the nearby nuclear spins is essential for the function of a chemical compass. We introduce an operationally defined measure for this kind of global electron-nuclear coherence to quantify its role in chemical magnetoreception, and demonstrate its direct connection with the magnetic sensitivity of a chemical compass. Our result offers a new perspective to understand how a variety of design principles will affect chemical magnetoreception, such as the hyperfine configurations, the nuclear spin polarizations and the different types of noise. It thus evidences that the chemical compass model of avian magnetoreception is similar to a coherence based quantum device, and provides us with a route to better understand the role of quantum effects in chemical magnetoreception. The verification of the present observation is conceivable either in spin chemistry experiments or by quantum simulation with well controllable systems [48] to emulate the radical pair dynamics.

[1] G. S. Engel, T. R. Calhoun, E. L. Read, T.-K. Ahn, T. Manal, Y.-C. Cheng, R. E. Blankenship, G. R. Fleming, *Evidence for wavelike energy transfer through quantum coherence in photosynthetic systems.* Nature **446**, 782-786 (2007).

[2] E. Collini, C. Y. Wong, K. E. Wilk, P. M. G. Curmi, P. Brumer, G. D. Scholes, *Coherently wired light-harvesting in photosynthetic marine algae at ambient temperature.* Nature 463, 644-647 (2010).

[3] M. Mohseni, P. Rebentrost, S. Lloyd, and A. Aspuru-Guzik, *Environment-assisted quantum walks in photosynthetic energy transfer.* J. Chem. Phys. **129**, 174106 (2008).

[4] M. B. Plenio and S. F. Huelga, *Dephasing-assisted transport: quantum networks and biomolecules*, New J. Phys. **10**, 113019 (2008).

[5] G. D. Scholes, G. R. Fleming, A. Olaya-Castro, and R. van Grondelle, *Lessons from nature about solar light harvesting.* Nature Chemistry **3**, 763774 (2011).

[6] A. W. Chin, J. Prior, R. Rosenbach, F. Caycedo-Soler, S. F. Huelga, and M. B. Plenio, *The role of non-equilibrium vibrational structures in electronic coherence and recoherence in pigmentprotein complexes*, Nature Physics. **9**, 113-118 (2013).

[7] L. Turin, *A method for the calculation of odor character from molecular structure.* J. Theor. Biol. **216**(3), 367 (2002).

[8] J. C. Brookes, F. Hartoutsiou, A. P. Horsfield, and A. M. Stoneham, *Could humans recognize odour by phonon assisted tunneling?* Phys. Rev. Lett. **98**, 038101 (2007).

[9] I. A. Solov'yov, P.-Y. Chang, and K. Schulten, *Vibrationally assisted electron transfer mechanism of olfaction: myth or reality?* Phys. Chem. Chem. Phys. **14**, 13861-13871 (2012) .

[10] K. Schulten, C. E. Swenberg, and A. Weller, *A biomagnetic sensory mechanism based on magnetic field modulated coherent electron spin motion*, Z. Phys. Chem **NF111**, 1-5 (1978).

[11] T. Ritz, S. Adem, and K. Schulten, *A model for photoreceptor-based magnetoreception in birds.* Biophys. J. **78**, 707718 (2000).

[12] Ilia A. Solov'yov, D. Chandler, and K. Schulten, *Exploring the possibilities for radical pair effects in cryptochrome*, Biophys. J **92**, 2711 (2007).

[13] C.T. Rodgers and P.J. Hore, *Chemical magnetoreception in birds: The radical pair mechanism*, Proc. Natl. Acad. Sci. U.S.A. **106**, 353 (2009).

[14] T. Ritz, R. Wiltschko, P. J. Hore, C. T. Rodgers, K. Stapput, P. Thalau, C. R. Timmel, W. Wiltschko, *Magnetic Compass of Birds Is Based on a Molecule with Optimal Directional Sensitivity.* Biophys. J. **96**, 3451 (2009).

[15] T. Ritz, M. Ahmad, H. Mouritsen, R. Wiltschko, W. Wiltschko, *Photoreceptor-based magnetoreception: optimal design of receptor molecules, cells, and neuronal processing* , J. Royal. Soc. Interface **7**, S135-146 (2010).

[16] K. Maeda, K. B. Henbest, F. Cintolesi, I. Kuprov, C. T. Rodgers, P. A. Liddell, D. Gust, C. R. Timmel, P. J. Hore, *Chemical compass model of avian magnetoreception*, Nature **453**, 387-390 (2008).

[17] T. Ritz, *Quantum effects in biology: Bird navigation*, Procedia Chemistry **3**, 262 (2011).

[18] J. A. Jones, P.J. Hore, *Spin-selective reactions of radical pairs act as quantum measurements*, Chem. Phys. Lett. 488, 90 (2010).

[19] I. K. Kominis, *Quantum Zeno effect explains magnetic-sensitive radical-ion-pair reactions*, Phys. Rev. E **80**, 056115 (2009).

[20] J.-M. Cai, G. G. Guerreschi, and H. J. Briegel, *Quantum Control and Entanglement in a Chemical Compass*, Phys. Rev. Lett. **104**, 220502 (2010).

[21] E. M. Gauger, E. Rieper, J. J. L. Morton, S. C. Benjamin, and V. Vedral, *Sustained Quantum Coherence and Entanglement in the Avian Compass*, Phys. Rev. Lett. **106**, 040503 (2011).

[22] J.-M. Cai, F. Caruso, and M. B. Plenio, *Quantum limits for the magnetic sensitivity of a chemical compass*, Phys. Rev. A **85**, 040304 (2012).

[23] J. N. Bandyopadhyay, T. Paterek, and D. Kaszlikowski, *Quantum Coherence and Sensitivity of Avian Magnetoreception*, Phys. Rev. Lett. **109**, 110502 (2012).

[24] E. M. Gauger, S. C. Benjamin, *Comment on "Quantum Coherence and Sensitivity of Avian Magnetoreception"*, arXiv:1303.4539 (2013).

[25] H. J. Hogben, T. Biskup, and P. J. Hore, *Entanglement and Sources of Magnetic Anisotropy in Radical Pair-Based Avian Magnetoreceptors*, Phys. Rev. Lett. **109**, 220501 (2012).

[26] S. Johnsen and K. J. Lohmann, *The physics and neu-*

robiology of magnetoreception. Nature Rev. Neurosci. **6**, 703712 (2005).

[27] J. L. Kirschvink, *et al. Magnetite Biomineralization and Magnetoreception in Organisms*, (Plenum, New York, USA, 1985).

[28] H.J. Werner, Z. Schulten, and K. Schulten, *Theory of the magnetic field modulated geminate recombination of radical ion pairs in polar solvents: Application to the pyreneN,Ndimethylaniline system.* J. Chem. Phys. **67**, 646 (1977).

[29] U.E. Steiner, T. Ulrich, *Magnetic Field Effects in Chemical Kinetics and Related Phenomena*, Chem. Rev. **89**, 51 (1989).

[30] H. Mouritsen, U. Janssen-Bienhold, M. Liedvogel, G. Feenders, J. Stalleicken, P. Dirks, R. Weiler, *Cryptochromes and neuronal-activity markers colocalize in the retina of migratory birds during magnetic orientation.* Proc. Natl Acad. Sci. USA **101**, 1429414299 (2004).

[31] J. C. Weaver, T. E. Vaughan and R. D. Astumian, *Biological sensing of small field differences by magnetically sensitive chemical reactions.* Nature **405**, 707709 (2000).

[32] F. Cintolesi, T. Ritz, C. W. M. Kay, C. R. Timmel and P. J. Hore, *Anisotropic recombination of an immobilized photoinduced radical pair in a 50-mT magnetic field: A model avian photomagnetoreceptor.* Chem. Phys. **294**, 385399 (2003).

[33] I. A. Solovyov, D. E. Chandler and K. Schulten, *Magnetic field effects in Arabidopsis thaliana cryptochrome-1.* Biophys. J. **92**, 27112726 (2007).

[34] M. Ahmad, P. Galland, T. Ritz, R. Wiltschko and W. Wiltschko, *Magnetic intensity affects cryptochrome-dependent responses in Arabidopsis thaliana.* Planta **225**, 615624 (2007).

[35] M. Zapka, D. Heyers, C. M. Hein, S. Engels, N.-L. Schneider, J. Hans, S. Weiler, D. Dreyer, D. Kishkinev, J. M. Wild, H. Mouritsen, *Visual but not trigeminal mediation of magnetic compass information in a migratory bird*, Nature **461**, 1274-1277 (2009).

[36] K. Maeda, A.J. Robinson, K.B. Henbest, H.J. Hogben, T. Biskup, M. Ahmad, E. Schleicher, S. Weber, C.R. Timmel, and P.J. Hore, *Magnetically sensitive light-induced reactions in cryptochrome are consistent with its proposed role as a magnetoreceptor*, Proc. Natl. Acad. Sci. U.S.A. 109, 4774 (2012).

[37] I. A. Solov'yov, H. Mouritsen, K. Schulten, *Acuity of a Cryptochrome and Vision-Based Magnetoreception System in Birds*, Biophy. J. **99**, 40-49 (2010).

[38] I. A. Solov'yov, T. Domratcheva, A. R. M. Shahi, and K. Schulten, *Decrypting cryptochrome: Revealing the molecular identity of the photoactivation reaction.* Journal of the American Chemical Society. **134**, 8046-1805 (2012).

[39] J. B Phillips, and S. C. Borland, *Behavioural evidence for use of a light-dependent magnetoreception mechanism by a vertebrate.* Nature **359**, 142144 (1992).

[40] W. Wiltschko, R. Wiltschko, *Magnetic orientation and magnetoreception in birds and other animals.* J. Comp. Physiol. A. **191**, 675-693 (2005).

[41] T. Ritz, P. Thalau, J. B. Phillips, R. Wiltschko and W. Wiltschko, *Resonance effects indicate a radical-pair mechanism for avian magnetic compass.* Nature **429**, 177180 (2004).

[42] D. Budker, and M. Romalis, *Optical magnetometry*, Nature Physics **3**, 227 - 234 (2007).

[43] J. R. Maze *et al*, *Nanoscale magnetic sensing with an individual electronic spin in diamond*, Nature **455**, 644 (2008).

[44] G. Balasubramanian *et al*, *Nanoscale imaging magnetometry with diamond spins under ambient conditions*, Nature **455**, 648 (2008).

[45] O. Efimova and P. J. Hore, *Role of Exchange and Dipolar Interactions in the Radical Pair Model of the Avian Magnetic Compass*, Biophys. J., **94**, 1565-1574 (2008).

[46] To explore the essential features of typical radical pair molecules, in the present work, rather than looking at radical pairs with very specific hyperfine configurations [21–25], we consider the realistic radical pairs in total consist of more than three up to seven nuclei with random hyperfine interaction strengths on the order of $\sim$ mT, see e.g. [32]. Besides the typical behaviors of general radical pair molecules, particularly, we also take the flavin-superoxide radical pair, which is a proposed candidate for avian magnetoreception [14, 15], as a representative example to further elaborate our results.

[47] J.-M. Cai, F. Jelezko, M. B. Plenio, A. Retzker, *Diamond based single molecule magnetic resonance spectroscopy.* New J. Phys. **15**, 013020 (2013).

[48] J.-M. Cai, A. Retzker, F. Jelezko, M. B. Plenio, *A large-scale quantum simulator on a diamond surface at room temperature.* Nature Physics **9**, 168173 (2013).

[49] P. London, J. Scheuer, J.-M. Cai, I. Schwarz, A. Retzker, M.B. Plenio, M. Katagiri, T. Teraji, S. Koizumi, J. Isoya, R. Fischer, L. P. McGuinness, B. Naydenov, and F. Jelezko, *Detecting and polarizing nuclear spins with double resonance on a single electron spin.* Submitted (2013).

[50] A. I. Shushin, *The effect of the spin exchange interaction on SNP and RYDMR spectra of geminate radical pairs.* Chem. Phys. Lett. **181**, 274-278 (1991).

Supplementary Information

The hyperfine couplings for the nuclei in the flavin radical.— The flavin-superoxide radical pair is the postulated candidate system responsible for avian magnetoreception, the structure of which [S1] is shown in Fig.1. The isotropic hyperfine coupling constants (a_{iso}), the principal values of the anisotropic part of the hyperfine tensors (T_{ii}, with $i = 1, 2, 3$) and the principal hyperfine axes for nuclei in the flavin (FADH$^\bullet$) radical that we use to calculate the results for the flavin-superoxide radical pair in both the main text and the following section of this supplementary information is based on the data in [S1], see Table I, which include the five nuclei with the largest isotropic hyperfine couplings and/or the largest anisotropy.

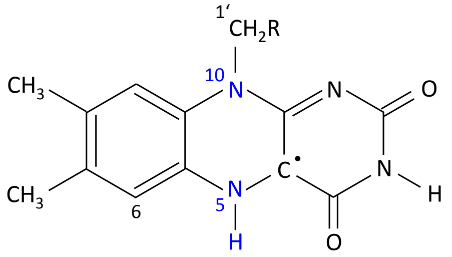

FIG. 1: **The structure of the flavin radical FADH$^\bullet$**. The most significant hyperfine interactions in FADH$^\bullet$ are from the nitrogen N5 and N10, and the proton H5 (blue).

TABLE I: hyperfine couplings for the nuclei in the flavin radical FADH$^\bullet$

Nucleus	a_{iso}(mT)	T_{ii}(mT)	Principal hyperf axes		
N5	0.393	0.498	0.4380	0.8655	0.2432
		0.492	0.8981	0.4097	0.1595
		0.989	0.0384	0.2883	0.9568
H5	0.769	0.616	0.9819	0.1883	0.0203
		0.168	0.0348	0.2850	0.9579
		0.784	0.1861	0.9398	0.2864
N10	0.212	0.242	0.9703	0.2207	0.0992
		0.234	0.2383	0.9426	0.2340
		0.476	0.0419	0.2506	0.9672
H1′r	0.390	0.062	0.1902	0.3965	0.8981
		0.033	0.9156	0.4017	0.0165
		0.095	0.3542	0.8255	0.4395
H6	0.158	0.060	0.0362	0.2937	0.9552
		0.044	0.7948	0.5879	0.1507
		0.104	0.6059	0.7537	0.2546

The basics of quantum metrology.— In a quantum interferometer, see Fig.1a in the main text, the system is prepared in a general state written as

$$\rho_0 = |\Psi_0\rangle\langle\Psi_0|, \quad \text{with} \quad |\Psi_0\rangle = \gamma_\alpha|\alpha\rangle + \gamma_\beta|\beta\rangle, \tag{1}$$

when e.g. a photon going through a beam splitter or a $\frac{\pi}{2}$ pulse is applied on a spin. The measurement-after-interference is given by the observable $\mathcal{M} = |\Psi_0\rangle\langle\Psi_0|$, and the interference fringe is

$$m_\lambda(\rho_0, \Phi_\lambda) = \mathrm{Tr}\left(\rho_{\Phi_\lambda}\mathcal{M}\right) = 1 - 2|\gamma_\alpha|^2|\gamma_\beta|^2\left(1 - \cos\Phi_\lambda\right). \tag{2}$$

The precision of parameter estimation with such a basic quantum interferometer is determined by the contrast of the interference fringe as defined in the following

$$\mathrm{D}_{\vec{\gamma}}(\rho_0) \equiv \max_{\Phi_\lambda} m_\lambda(\rho_0, \Phi_\lambda) - \min_{\Phi_\lambda} m_\lambda(\rho_0, \Phi_\lambda) = 2|\gamma_\alpha|^2|\gamma_\beta|^2 \equiv \gamma. \tag{3}$$

The contrast of the interference fringe $\mathrm{D}_{\vec{\gamma}}(\rho_0)$ illustrates how coherent the quantum interferometer is, as seen in Fig.2(a-b), the more coherence, the larger the interference contrast and thus the better the precision of parameter estimation for quantum metrology [S2, S3]. We remark that the quantification of the role of coherence in a quantum interferometer-based metrology as given in Eq.(4) of the main text is is operational and connects coherence to metrological precision, and thus is more preferable than the simple summation of the absolute values of the off-diagonal density matrix elements, although these two measures are identical for the present observable $\mathcal{M} = |\Psi_0\rangle\langle\Psi_0|$. However, they may not be equivalent for general observables. The key point being that our measure of coherence does not merely consider a state but is operationally defined as it takes account of the dynamics of the system (from the hyperfine interactions of the radical pair) and the measurement procedure too. Having introduced the basics of quantum metrology, we list in Table II the analogies between a quantum interferometer and a chemical compass that are relevant for the function of a quantum coherence device, which provide us inspirations to characterize the role of coherence in chemical magnetoreception.

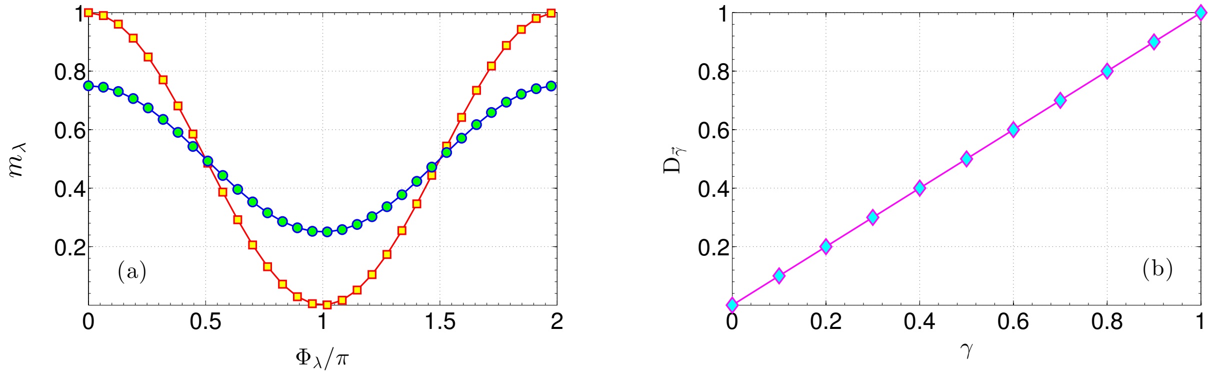

FIG. 2: **(a)**: The interference fringe of a quantum interferometer m_b as a function of the phase Φ_b with the value of $\gamma \equiv 2|\gamma_\alpha|^2|\gamma_\beta|^2 = 1$ (red, square) and 0.5 (blue, circle). **(b)**: The contrast of the interference fringe D_γ as a function of γ.

TABLE II: Analogy between a quantum interferometer and chemical compass model

	Quantum Interferometer	*Chemical Compass model*
Basis	Interference paths	Eigenstates of hyperfine interaction Hamiltonian
Observable	$\mathcal{M} = \lvert\Psi_0\rangle\langle\Psi_0\rvert$	Spin-dependent reactions $\mathcal{M} = ke^{-kt}(\lvert\mathcal{S}\rangle\langle\mathcal{S}\rvert \otimes_{k_j} \mathbb{I}_{d_{k_j}})$
Outcome	$m_\lambda(\rho_0, \Phi_\lambda)$: Eq.(3)	Singlet yield $\mathrm{Y_S}(\mathcal{H}_0, \rho_0, \theta, \varphi)$: Eq.(11)
Sensitivity	Interference fringe contrast $\mathrm{D}_{\vec{\gamma}}(\rho_0)$: Eq.(4)	Magnetic anisotropy of singlet yield $\mathrm{D_S}(\mathcal{H}_0, \rho_0)$: Eq.(12)
Coherence	$\mathcal{C} = \lvert m_\lambda(\rho_0^c, \Phi_\lambda)\rvert_{\Phi_\lambda=0}$: Eq.(5)	$\mathcal{C}(\mathcal{H}_0, \rho_0) = \lvert\mathrm{Y_S}(\mathcal{H}_0, \mathcal{GC}(\mathcal{H}_0, \rho_0))\rvert_{b=0}$: Eq.(14)

The effective evolution of a chemical compass.— The system state of the radical pair and nuclear spins ρ_0, written in the eigenbasis $\{|\nu_m\rangle\}$ of the Hamiltonian $\mathcal{H}_0$, can be expressed as

$$\rho_0 = \sum_{m,n} r_{mn}|\nu_m\rangle\langle\nu_m|, \quad \text{with} \quad r_{mn} = \langle\nu_m|\rho_0|\nu_n\rangle. \tag{4}$$

To show that for a typical radical pair molecule with a few nuclei, where the external magnetic field (much smaller than the hyperfine interactions) can be treated as a perturbation, its effect is mainly to introduce an additional phase on the system coherence, namely

$$\rho(t) \equiv \rho^{\mathcal{H}_0+\hat{\mathrm{B}}(\theta,\varphi)}(t) \approx \sum_{m,n} r_{mn}(t)e^{-i\left[\varphi^0_{mn}(t)+\varphi^b_{mn}(t)\right]}|\nu_m\rangle\langle\nu_n|, \tag{5}$$

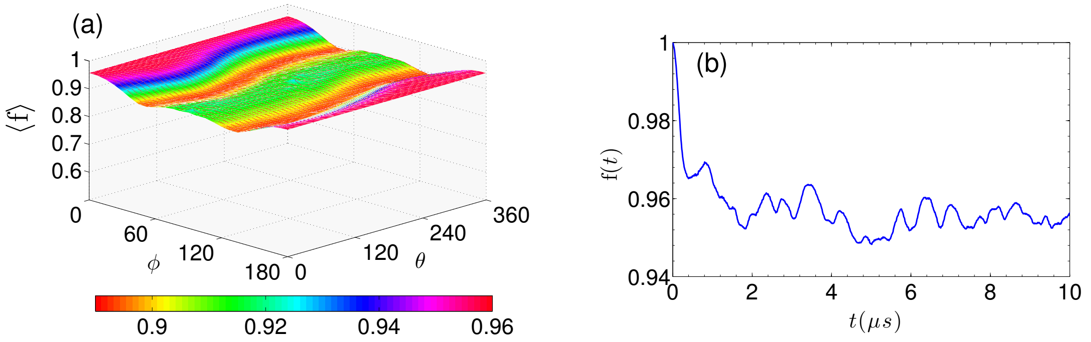

FIG. 3: **(a)** The fidelity (averaging over time) as defined in Eq.(7) between the system state $\rho(t) \equiv \rho^{\mathcal{H}_0+\hat{\mathrm{B}}(\theta,\varphi)}(t)$ and the corresponding state neglecting the change of the absolute values of the density matrix elements for the flavin-superoxide radical pair with different magnetic field directions (θ,φ). **(b)** The fidelity $\mathrm{f}(t)$ as a function of time t for the specific magnetic field direction $(\theta,\varphi)=(0,0)$. The strength of the magnetic field is $b=50\mu T$.

see Eq.(8-10) in the main text, we use the following quantity

$$\epsilon(t)=\sqrt{\sum_{m\neq n}\left(r_{mn}^{t}-r_{mn}\right)^2} \tag{6}$$

to demonstrate that the weak magnetic field would only slightly change the absolute values of the density matrix elements when written in the eigenbasis of the hyperfine interaction Hamiltonian $\mathcal{H}_0$, see Fig.2(a) in the main text. The calculation is done for the flavin-superoxide radical pair in cryptochrome protein, and the hyperfine coupling consists of 2 nitrogen (spin-1) and 3 hydrogen (spin-$\frac{1}{2}$) nuclear spins, see Table I [S1]. Here, we further support the observation by using another quantity to show the slight change in the absolute values of the density matrix elements as

$$\mathrm{f}(\rho(t),\rho_{\mathrm{C}}(t))=\mathrm{Tr}\sqrt{\sqrt{\rho_{\mathrm{C}}(t)}\,\rho(t)\sqrt{\rho_{\mathrm{C}}(t)}}, \tag{7}$$

which defines the fidelity between the system state $\rho(t) \equiv \rho^{\mathcal{H}_0+\hat{\mathrm{B}}(\theta,\varphi)}(t)$ (under the evolution governed by the total Hamiltonian $\mathcal{H}=\mathcal{H}_0+\hat{\mathrm{B}}(\theta,\varphi)$) and the corresponding state neglecting the change in the absolute values of the density matrix elements as

$$\rho_{\mathrm{C}}(t)=\sum_{m,n} r_{mn}e^{-i\left[\varphi^{0}_{mn}(t)+\varphi^{b}_{mn}(t)\right]}|\nu_m\rangle\langle\nu_n|. \tag{8}$$

In Fig.3, we plot the average value of $\langle \mathrm{f}(\rho(t),\rho_{\mathrm{C}}(t))\rangle$ for the magnetic field with different directions (θ,φ). It can be seen that the fidelity is very close to 1, which indicates that the change in the absolute values of the density matrix elements is very small.

Nuclear spin polarization and the magnetic sensitivity of a chemical compass.— In this section we would like to compare the magnetic sensitivity with a polarized and unpolarized nuclear environment to provide further evidence that the global electron-nuclear coherence is a meaningful coherence measure. To this end, we use the flavin-superoxide radical pair as an example and compare the magnetic sensitivity from the depolarized and polarized nuclear spin initial states, see Fig.4. The improvement of the magnetic sensitivity can be attributed to the enhancement of the global electron-nuclear spin coherence as measured by $\mathcal{C}(\mathcal{H}_0,\rho_0)=|\mathrm{Y}_{\mathrm{S}}(\mathcal{H}_0,\mathcal{GC}(\mathcal{H}_0,\rho_0))|_{b=0}$, see Eq.(14) in the main text, which increases from 0.105 to 0.2. More generally, the concept of global electron-nuclear spin coherence make it possible to understand the effect of nuclear polarization on the magnetic sensitivity of a chemical compass straightforwardly. It should be noted that with the techniques of chemical-induced dynamical nuclear spin polarization or appropriate quantum control technologies [S4, S5] (partial) polarization of the nuclear spins is possible and thus this comparison is also conceivable with current experimental technology.

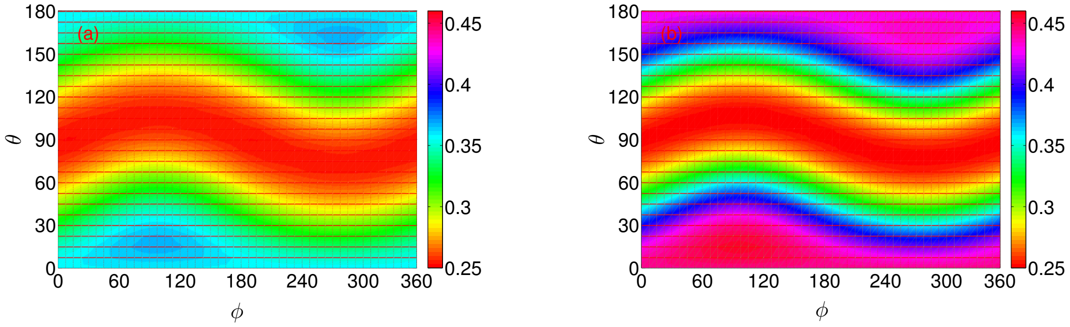

FIG. 4: **Nuclear spin polarization and magnetic sensitivity of the flavin-superoxide radical pair.** The dependence of the singlet yield $\mathrm{Y_S}(\mathcal{H}_0, \rho_0, \theta, \varphi)$ on the magnetic field direction (θ, φ) of the flavin-superoxide radical pair with the depolarized **(a)** and polarized **(b)** nuclear spin initial state. The common parameters for both panels are: the strength of the magnetic field is $b = 50\mu T$, and the reaction rates are $k_S = k_T = 0.5\mu s^{-1}$.

Dynamic features of the the global electron-nuclear spin coherence.— The system state of the radical pair and nuclear spins ρ_0, written in the eigenbasis $\{|\nu_m\rangle\}$ of the Hamiltonian $\mathcal{H}_0$, can be expressed as

$$\rho_0 = \sum_{m,n} r_{mn} |\nu_m\rangle\langle\nu_m|, \quad \text{with} \quad r_{mn} = \langle\nu_m|\rho_0|\nu_n\rangle. \tag{9}$$

In the absence of a magnetic field, the state evolution is as

$$\rho^{\mathcal{H}_0}(t) = \sum_{m,n} r_{mn} e^{-i\varphi^0_{mn}(t)} |\nu_m\rangle\langle\nu_n|. \tag{10}$$

We stress that the definition of the global electron-nuclear spin coherence is only based on the system dynamics without a magnetic field, it is thus *not* a representation of the system dynamics under the action of the weak magnetic field (e.g. the Earth's magnetic field). In Fig.4 of the main text, we demonstrate that the effects of different noises can be understood in a unified picture by looking at how each type of noise destroys the global electron-nuclear spin coherence. Here we illustrate the decoherence effects in more details by looking at the dynamical features. With a

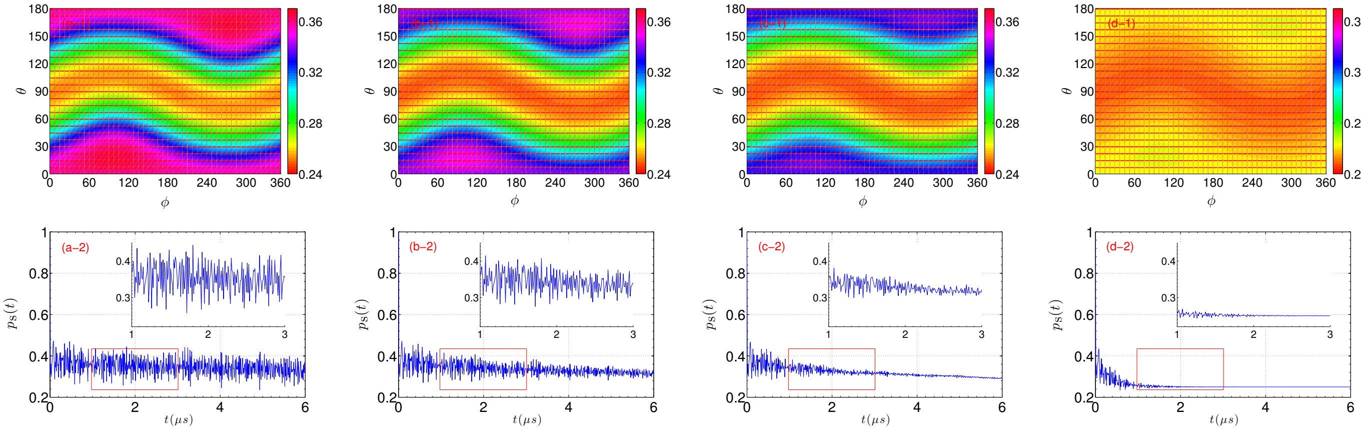

FIG. 5: **Upper panels**: The dependence of the singlet yield $\mathrm{Y_S}(\mathcal{H}_0, \rho_0, \theta, \varphi)$ on the magnetic field direction (θ, φ) of the flavin-superoxide radical pair under different types of decoherence: without noise **(a-1)**, the local dephasing model **(b-1)**, the spin relaxation **(c-1)**, and the singlet-triplet dephasing model **(d-1)**. **Lower panels**: The singlet fraction (in the state evolution $\rho^{\mathcal{H}_0}(t)$ that is only governed by the hyperfine interaction, namely *without* the magnetic field) as a function of time t for different types of decoherence: without noise **(a-2)**, the local dephasing model **(b-2)**, the spin relaxation **(c-2)**, and the singlet-triplet dephasing model **(d-2)**. The insets show the zoom in of the time regime $[1\mu s, 3\mu s]$in the red box. The strength of the magnetic field is $b = 50\mu T$, and the reaction rates are $k_S = k_T = 0.5\mu s^{-1}$.

same decoherence rate ξ, different noise models disrupt the magnetic sensitivity in varying degrees. In Fig.5(a-1,b-1,c-1,d-1), we choose $\xi = 0.4\mu s^{-1}$ as an example, and plot the dependence of the singlet yield on the magnetic field direction (θ, φ) for different types of decoherence. The global electron-nuclear spin coherence is manifested by the oscillations of the singlet fraction

$$p_{\mathrm{S}}(t) = \langle \mathcal{S}|\rho^{\mathcal{H}_0}(t)|\mathcal{S}\rangle = \sum_{m,n} r_{mn} e^{-i\varphi^0_{mn}(t)} \langle \nu_n|\mathcal{S}\rangle\langle \mathcal{S}|\nu_m\rangle. \tag{11}$$

The decoherence effects on the oscillations of the singlet fraction (in the state evolution $\rho^{\mathcal{H}_0}(t)$ that is only governed by the hyperfine interaction) are also plotted in Fig.5(a-2,b-2,c-2,d-2), which evidence how they destroy the global electron-nuclear spin coherence, and thereby decrease the magnetic sensitivity when adding a weak magnetic field.

Random configurations of hyperfine couplings with nuclei.— The hyperfine coupling tensor with one nuclear spin is parametrized by the isotropic hyperfine coupling constants (a_{iso}), the principal values of the anisotropic part of the hyperfine tensors (T_{ii}, with $i = 1; 2; 3$) and the three orthogonal principal hyperfine axes $(\hat{n}^k_x, \hat{n}^k_y, \hat{n}^k_z)$ with $k = 1; 2; 3$, e.g. see Table I. In our random sampling, the values of a_{iso}, T_{ii} and $(\hat{n}^k_x, \hat{n}^k_y, \hat{n}^k_z)$ are generated randomly under the realistic constraints: $|a_{iso}| \leq 1\mathrm{mT}$, $|T_{11}| \leq 1\mathrm{mT}$, $|T_{22}| \leq 1\mathrm{mT}$, and $T_{33} = T_{11} + T_{22}$.

The differentiation between global electron-nuclear spin coherence and local electron-spin coherence.— In the main text, we investigate the role of coherence with the concept of global electron-nuclear spin quantum coherence, which is essentially different from the conventional definition of local electron-spin quantum coherence. In this section of supplementary information, we give more explicit definitions for these two kinds of coherence, and further illustrate their contributions to chemical magnetoreception in the next section. The concept of quantum coherence arises from the basic principle of quantum mechanics, namely a quantum system can be in a *superposition* of different orthogonal states (called as a set of basis states). Quantum coherence of a given state can be uniquely defined only when a set of basis states are specified. Expressed in a specific set of basis, the off-diagonal density matrix elements of a quantum state represent its coherent properties. In the case where the radical pair is born in the singlet state and the nuclei are depolarized, the system (including the radical pair and the nearby nuclei) state is

$$\rho_0 = |\mathcal{S}\rangle\langle\mathcal{S}| \bigotimes_{k_j} \left(\mathbb{I}_{d_{k_j}}/d_{k_j}\right) \tag{12}$$

where d_{k_j} is the dimension of the k_jth nuclear spin, $\mathbb{I}_{d_{k_j}}$ is the $d_{k_j} \times d_{k_j}$ identity matrix, and $|\mathcal{S}\rangle = \sqrt{\frac{1}{2}}\left(|\alpha\beta\rangle - |\beta\alpha\rangle\right)$ is the singlet radical pair state. Written in the conventional local spin basis $\{|\alpha\rangle, |\beta\rangle\}$, the above state has non-zero

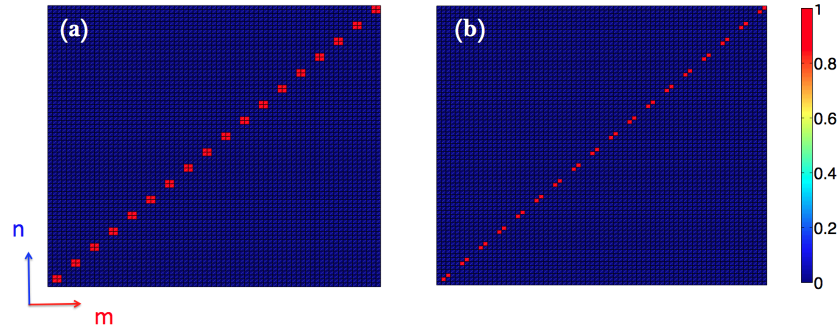

FIG. 6: **The illustration of the state of the combined system of the radical pair and the nearby nuclei**. The density matrix elements $|(\rho_0)\mathrm{mn}|$ (with ρ_0 written in Eq.(13)) **(a)** in the local electron spin basis and **(b)** the corresponding state, see Eq.(14), by vanishing the local electron spin coherence. For better visibility, the absolute values of the density matrix elements are normalized by the largest element.

off-diagonal density matrix elements (namely local electron-spin quantum coherence)

$$\rho_0 = \frac{1}{2}\begin{pmatrix} 0 & 0 & 0 & 0 \\ 0 & 1 & -1 & 0 \\ 0 & -1 & 1 & 0 \\ 0 & 0 & 0 & 0 \end{pmatrix} \bigotimes_{k_j} \frac{1}{d_{k_j}} \begin{pmatrix} 1 & 0 & \cdots & 0 \\ 0 & 1 & \cdots & 0 \\ \vdots & \vdots & \ddots & \vdots \\ 0 & 0 & \cdots & 1 \end{pmatrix}_{d_{k_j}\times d_{k_j}} . \tag{13}$$

The corresponding incoherent state by vanishing its local quantum coherence, namely the off-diagonal density matrix elements as in Eq.(13) is (see Fig.6a)

$$\mathbb{IC}_{\mathcal{L}}(\rho_0) = \frac{1}{2}\begin{pmatrix} 0 & 0 & 0 & 0 \\ 0 & 1 & 0 & 0 \\ 0 & 0 & 1 & 0 \\ 0 & 0 & 0 & 0 \end{pmatrix} \bigotimes_{k_j} \frac{1}{d_{k_j}} \begin{pmatrix} 1 & 0 & \cdots & 0 \\ 0 & 1 & \cdots & 0 \\ \vdots & \vdots & \ddots & \vdots \\ 0 & 0 & \cdots & 1 \end{pmatrix}_{d_{k_j}} . \tag{14}$$

The definition of local quantum coherence is thus not dependent on the hyperfine coupling properties of individual radical pair molecules, based on which it is not likely to enable us to make a general statement on the role of quantum coherence in chemical magnetoreception for different radical pair molecules, see e.g. Ref.[S6].

Given an example of radical pair with the hyperfine interaction Hamiltonian $\mathcal{H}_0$, the eigenbasis of which are denoted as $\{|\nu_m\rangle\}$, the radical pair state can instead be written in the eigenbasis as follows

$$\rho_0 = \sum_{m,n} r_{mn} |\nu_m\rangle\langle\nu_n|, \quad \text{with} \quad r_{mn} = \langle\nu_m|\rho_0|\nu_n\rangle. \tag{15}$$

where $\{|\nu_m\rangle\}$ are the eigenstates of the hyperfine interaction $\mathcal{H}_0$. We call the coherence in this representation as global electron-nuclear spin coherence, which is abbreviated as quantum coherence without causing confusion in the main text. The coherence properties by this definition depends on both the system state and the hyperfine interactions in individual molecules. The concept of global electron-nuclear spin coherence is different from local electron-spin coherence. In particular, even the local incoherent state $\mathbb{IC}_{\mathcal{L}}(\rho_0)$, see Eq.(14), may exhibit a certain level of global quantum coherence, see an example in Fig.7. In contrast, the global incoherent state corresponding to a system state ρ_0 as defined in the following

$$\mathbb{IC}_{\mathcal{G}}(\mathcal{H}_0, \rho_0) = \sum_{m} r_{mm} |\nu_m\rangle\langle\nu_m|, \quad \text{with} \quad r_{mm} = \langle\nu_m|\rho_0|\nu_m\rangle. \tag{16}$$

does not have global quantum coherence.

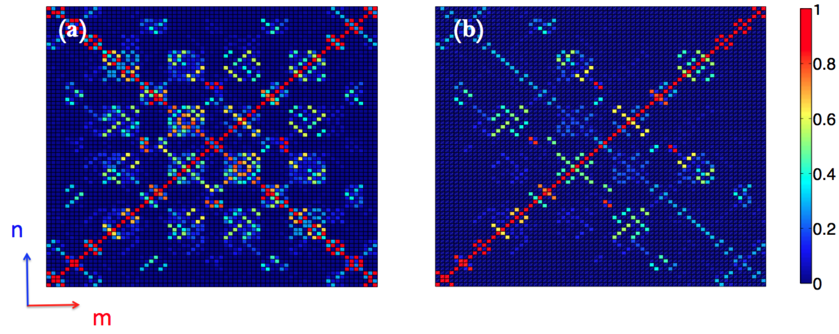

FIG. 7: **The illustration of the state of the combined system of the radical pair and the nearby nuclei**. The density matrix elements $|(\rho_0)\mathrm{mn}|_{|\nu_m\rangle,|\nu_n\rangle}$ **(a)** in the eigenbasis of the hyperfine interaction Hamiltonian $\mathcal{H}_0$ (with three nuclear spins that have the largest anisotropy of hyperfine couplings (namely N5, H5, N10, see Table I) in the flavin-superoxide radical pair) and **(b)** the corresponding state, see Eq.(14), by vanishing the local electron spin coherence. For better visibility, the absolute values of the density matrix elements are normalized by the largest element.

The contributions of global electron-nuclear spin coherence and local electron-spin coherence to the magnetic sensitivity.— In the previous studies on the role of quantum coherence (or an extended concept of quantum entanglement) in a chemical compass, work usually focused on local radical pair electron-spin coherence. In the main text, we introduce the notion of global electron-nuclear spin coherence (see also the previous section), and show that it is essential for the function of a chemical compass. Here, we compare the contributions of both local and global electron-nuclear spin coherence to the magnetic sensitivity of a chemical compass, to provide further support for our observation that global electron-nuclear spin coherence is a more fruitful concept allowing us to characterize the role of coherence in chemical magnetoreception. We numerically sample a number of hyperfine coupling configurations with from three up to six nuclei, and we assume that the radical pair is born in the singlet so that the initial system state is $\rho_0 = |\mathcal{S}\rangle\langle\mathcal{S}| \otimes_{k_j} \left(\mathbb{I}_{k_j}/d_{k_j}\right)$. The contribution of the global electron-nuclear spin coherence to the magnetic sensitivity is defined as

$$f^{\mathcal{GC}}(\mathrm{D_S}) = \langle \mathrm{D_S}(\mathcal{H}_0, \mathcal{GC}(\mathcal{H}_0,\rho_0))/\mathrm{D_S}(\mathcal{H}_0,\rho_0)\rangle = 1 - \langle \mathrm{D_S}(\mathcal{H}_0, \mathbb{IC}_{\mathcal{G}}(\mathcal{H}_0,\rho_0))/\mathrm{D_S}(\mathcal{H}_0,\rho_0)\rangle, \tag{17}$$

where $\mathcal{GC}(\mathcal{H}_0,\rho_0) = \sum_{m\neq n} r_{mn}|\nu_m\rangle\langle\nu_n|$, $\mathbb{IC}_{\mathcal{G}}(\mathcal{H}_0,\rho_0) = \sum_m r_{mm}|\nu_m\rangle\langle\nu_m|$, with $r_{mn} = \langle\nu_m|\rho_0|\nu_n\rangle$, see Eq.(16). In contrast, the contribution of the local electron-spin coherence is

$$f^{\mathcal{LC}}(\mathrm{D_S}) = 1 - \langle \mathrm{D_S}(\mathcal{H}_0, \mathbb{IC}_{\mathcal{L}}(\rho_0))/\mathrm{D_S}(\mathcal{H}_0,\rho_0)\rangle, \tag{18}$$

where $\mathbb{IC}_{\mathcal{L}}(\rho_0)$ is the local incoherent state, see Eq.(14).

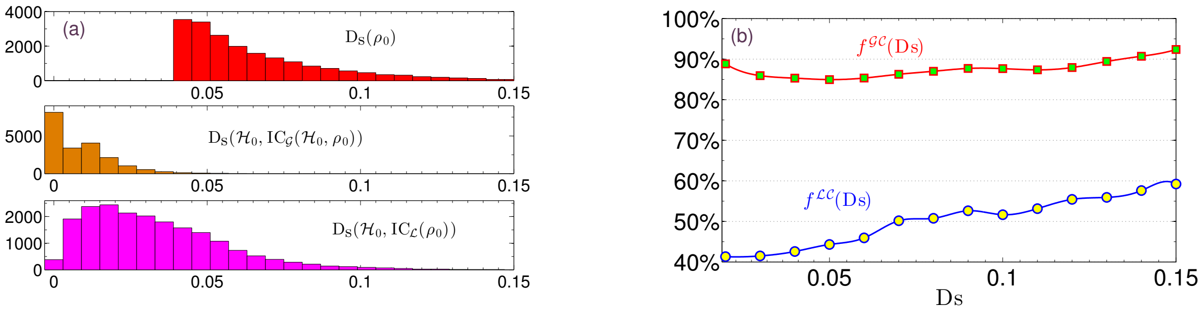

FIG. 8: **(a)** The histogram of the magnetic sensitivity $\mathrm{D_S}(\rho)$ **(upper)** that is larger than 0.04, and the magnetic sensitivity from the corresponding system state with vanishing global electron-nuclear spin coherence $\mathrm{D_S}(\mathcal{H}_0, \mathbb{IC}_{\mathcal{L}}(\rho_0))$ **(middle)** and with vanishing local electron-spin quantum coherence $\mathrm{D_S}(\mathcal{H}_0, \mathbb{IC}_{\mathcal{G}}(\rho_0))$ **(lower)** respectively. **(b)** The percentage of the magnetic sensitivity contributed by the local electron spin coherence and the global electron-nuclear spin coherence quantified by $f^{\mathcal{LC}}(\mathrm{D_S})$ and $f^{\mathcal{LC}}(\mathrm{D_S})$ respectively (see the definitions in Eq.(17,18)), averaging over the samples with $\mathrm{D_S}(\rho_0) \in [\mathrm{D_S}, \mathrm{D_S} + 0.01)$. In both panels, the hyperfine couplings are randomly sampled with in total 3-6 nuclear spins; the reaction rates are $k_S = k_T = 0.5\mu s^{-1}$ and the strength of the magnetic field is $b = 50\mu T$.

In Fig.8(a), we compare the magnetic sensitivity of a chemical compass with the ones excluding local electron-spin coherence (namely with the system state $\mathbb{IC}_{\mathcal{L}}(\rho_0)$, see Eq.(14)) and excluding the global electron-nuclear spin coherence (namely with the system state $\mathbb{IC}_{\mathcal{G}}(\rho_0)$, see Eq.(16)). It can be seen that the magnetic sensitivity can still be very high if the local electron-spin coherence is absent. Instead, the magnetic sensitivity significantly reduces when the global electron-nuclear spin coherence is absent. In Fig.8(b), we plot the contribution of coherence to the magnetic sensitivity, as quantified respectively by $f^{\mathcal{GC}}(\mathrm{D_S})$, see Eq.(17), and $f^{\mathcal{LC}}(\mathrm{D_S})$, see Eq.(18), by averaging over the samples with $\mathrm{D_S}(\rho_0) \in [\mathrm{D_S}, \mathrm{D_S} + \Delta)$. The results show that $f^{\mathcal{GC}}(\mathrm{D_S})$ is above 85% and much larger than $f^{\mathcal{LC}}(\mathrm{D_S})$, which clearly evidences the essential role of the global electron-nuclear spin coherence in chemical magnetoreception.

Haberkorn master equation for the radical pair dynamics.— To derive the Haberkorn master equation, we introduce the notation of $|e\rangle$, $|g\rangle$ to denote the radical pairs when they are excited or in the ground state respectively. In the conventional picture, we usually only deal with the excited radical pair state. One can write the system total Hamiltonian as follows

$$\mathcal{H}_{eg} = \mathcal{H} \bigotimes |e\rangle\langle e| = \left[\mathcal{H}_0 + \hat{\mathrm{B}}(\theta,\varphi)\right] \bigotimes |e\rangle\langle e|, \tag{19}$$

where $\mathcal{H}_0$ represents the hyperfine interactions. We note that the hyperfine coupling and the interaction with the magnetic field do not take effect if the molecule is in the ground state $|g\rangle$. The reaction channels from the singlet and triplet radical pair are represented by the following Lindblad operators

$$\begin{aligned} L_S &= Q_S \bigotimes |g\rangle\langle e|, & (20)\\ L_T &= Q_T \bigotimes |g\rangle\langle e|, & (21) \end{aligned}$$

where Q_S and Q_T are the projectors into the singlet and triplet subspace respectively. Therefore the system dynamics can described the following master equation as

$$\frac{\mathrm{d}}{\mathrm{dt}}\rho_{eg} = -i[\mathcal{H}_{eg}, \rho_{eg}] + k_S\left(L_S\rho_{eg}L_S^\dagger - \frac{1}{2}L_S^\dagger L_S\rho_{eg} - \frac{1}{2}\rho_{eg}L_S^\dagger L_S\right) + k_T\left(L_T\rho_{eg}L_T^\dagger - \frac{1}{2}L_T^\dagger L_T\rho_{eg} - \frac{1}{2}\rho_{eg}L_T^\dagger L_T\right) \tag{22}$$

We define the projector into the excite state subspace as

$$P_e = \mathbb{I}\bigotimes |e\rangle\langle e| \tag{23}$$

and apply it to the master equation in Eq. (22), which leads to

$$\begin{aligned} \frac{\mathrm{d}}{\mathrm{dt}}\left(P_e\rho_{eg}P_e\right) &= -i[\mathcal{H}_{eg}, (P_e\rho_{eg}P_e)] & (24)\\ &- \frac{k_S}{2}\left[(Q_S\otimes|e\rangle\langle e|)\cdot(P_e\rho_{eg}P_e) + (P_e\rho_{eg}P_e)\cdot(Q_S\otimes|e\rangle\langle e|)\right]\\ &- \frac{k_T}{2}\left[(Q_T\otimes|e\rangle\langle e|)\cdot(P_e\rho_{eg}P_e) + (P_e\rho_{eg}P_e)\cdot(Q_T\otimes|e\rangle\langle e|)\right] \end{aligned}$$

We denote $P_e\rho_{eg}P_e = \rho_e\otimes|e\rangle\langle e|$, and obtain the Haberkorn master equation for ρ_e from Eq.(25) as follows

$$\frac{\mathrm{d}}{\mathrm{dt}}\rho_e = -i[\mathcal{H}, \rho_e] - \frac{k_S}{2}\left(Q_S\rho_e + \rho_e Q_S\right) - \frac{k_T}{2}\left(Q_T\rho_e + \rho_e Q_T\right) \tag{25}$$

where $\mathcal{H} = \mathcal{H}_0 + \hat{\mathrm{B}}(\theta,\varphi)$. We remark that the density matrix ρ_e is not trace preserving as it only accounts for the population of excited state. The singlet yield (i.e. the singlet ground state population) after time t can be calculated as

$$\mathrm{Y_S}(t) = \mathrm{Tr}\left[\left(Q_S\otimes|g\rangle\langle g|\right)\rho_{eg}(t)\right]. \tag{26}$$

From Eq. (22-25), it is easy to obtain the following dynamics equations for the singlet yield as

$$\frac{\mathrm{d}}{\mathrm{dt}}\mathrm{Y_S}(t) = k_S\mathrm{Tr}\left[Q_S\rho_e(t)\right]. \tag{27}$$

that is

$$\mathrm{Y_S} = k_S\int \mathrm{Tr}\left[Q_S\rho_e(t)\right]dt. \tag{28}$$

In the particular case of $k_S = k_T \equiv k$, the solution of $\rho_e(t)$ can be simplified by introducing the density matrix $\rho^{\mathcal{H}_0+\hat{\mathrm{B}}(\theta,\varphi)}(t)$, see Eq.(10) in the main text and Eq.(5), which is the state evolution governed by the system Hamiltonian $\mathcal{H} = \mathcal{H}_0 + \hat{\mathrm{B}}(\theta,\varphi)$ as

$$\frac{\mathrm{d}}{\mathrm{dt}}\rho^{\mathcal{H}_0+\hat{\mathrm{B}}(\theta,\varphi)}(t) = -i[\mathcal{H}, \rho^{\mathcal{H}_0+\hat{\mathrm{B}}(\theta,\varphi)}(t)]. \tag{29}$$

It can be seen from the master equation Eq.(25) that $\rho_e(t) = e^{-kt}\rho^{\mathcal{H}_0+\hat{\mathrm{B}}(\theta,\varphi)}(t)$. Therefore, the singlet yield in Eq.(28) can be obtained as follows (see also Eq.(11) in the main text)

$$\mathrm{Y_S}(\mathcal{H}_0, \rho_0, \theta, \varphi) = \int \mathrm{Tr}\left[\rho^{\mathcal{H}_0+\hat{\mathrm{B}}(\theta,\varphi)}(t)\mathcal{M}\right]dt, \tag{30}$$

with the observable

$$\mathcal{M} = ke^{-kt}(|\mathcal{S}\rangle\langle\mathcal{S}| \otimes_{k_j} \mathbb{I}_{d_{k_j}}), \tag{31}$$

which is the so-called exponential model [S7].

Generalizations to more general radical pair reactions.— In the main text, for simplicity, we have considered the scenarios that the reaction rate $k_S = k_T \equiv k$. In such a case, the coherence generated during the evolution is very small, see the above section of *The effective evolution of a chemical compass.* Our idea can also be generalized to the radical pair reactions with $k_S \neq k_T$ by mapping to a continuous type of quantum interferometer so that we can also incorporate the coherence generated during the evolution. To this end, we divide the total time evolution t into small intervals $[\Delta t, \Delta t, \cdots, \Delta t]$, the dynamics of a chemical compass model can be view as a sequence of quantum interference processes [— *free evolution for time* Δt— *spin dependent chemical reactions* —$]^N$ because the singlet fraction is continuously leading to reaction products, see Fig.9.

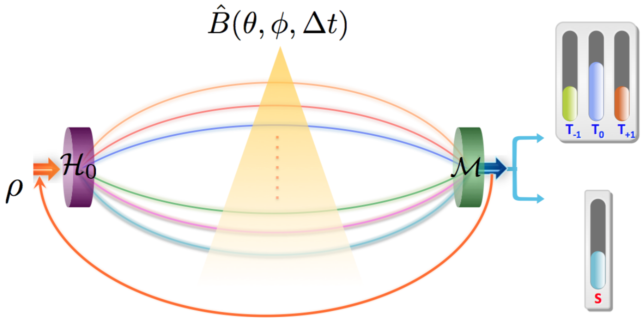

FIG. 9: **A continuous quantum interferometer model of chemical compass**. The dynamics of a general chemical compass is viewed as a sequence of quantum interference processes, the hyperfine coupling Hamiltonian $\mathcal{H}_0$ recasts the system state ρ into a superposition of its eigenstates. The weak magnetic field induces the change of coherence phases between different paths. The spin-dependent chemical reactions lead to the phase dependent observables. We refer the list of analogies between a quantum interferometer and a chemical compass to Table II .

The evolution of the system is described by the Haberkorn master equation [S7] as

$$\frac{\mathrm{d}}{\mathrm{dt}}\rho = -i[\mathcal{H}, \rho] - \frac{k_S}{2}[Q_S, \rho]_+ - \frac{k_T}{2}[Q_T, \rho]_+, \tag{32}$$

where $\mathcal{H} = \mathcal{H}_0 + \hat{\mathrm{B}}(\theta, \varphi)$ is the total Hamiltonian including the hyperfine couplings and the external magnetic field, Q_S and Q_T are the projectors into the singlet and triplet subspace individually, and $[x, y]_+ = xy + yx$, see also Eq.(25), here we simplify the notation ρ_e as ρ without causing confusion. The measure of coherence, in Eq.(13) of the main text, can then be generalized as

$$\mathcal{C}(\mathcal{H}_0, \rho_0) = |\int k_S \mathrm{Tr}\left[\mathcal{GC}(\mathcal{H}_0, \rho(t)) \cdot \mathcal{M}\right] dt|, \quad \text{with} \quad \mathcal{GC}(\mathcal{H}_0, \rho(t)) = \sum_{m \neq n} r_{mn}(t) |\nu_m\rangle\langle\nu_n|, \tag{33}$$

with $r_{mn}(t) = \langle\nu_m|\rho(t)|\nu_n\rangle$. The above quantity characterizes how coherent the corresponding quantum interference processes are. The corresponding measure of local electron-spin coherence is defined as

$$\mathcal{C}_{\mathcal{L}}(\rho_0) = |\int k_S \mathrm{Tr}\left[\mathcal{LC}(\rho(t)) \cdot \mathcal{M}\right] dt|, \tag{34}$$

with $\mathcal{LC}(\rho(t)) = \rho(t) - \mathbb{IC}_{\mathcal{L}}(\rho(t))$, see the definition in Eq.(14). Using this generalized measure to demonstrate the role of coherence in a general chemical compass, we first consider the flavin-superoxide radical pair as an example, and vary the ratio k_S/k_T while fixing the value of k_T. For the simplicity of calculations, we include three nuclear that have the largest anisotropy of hyperfine couplings (namely N5, H5, N10, see Table I). In Fig.10 (a_1), it can be seen that the magnetic sensitivity $\mathrm{D_S}$ changes with the ratio k_S/k_T, and in the extreme case of $k_S = 0$, obviously

$\mathrm{D_S} = 0$. The direct relation between the magnetic sensitivity $\mathrm{D_S}$ and the global electron-nuclear coherence $\mathcal{C}$, as defined in Eq.(33), is shown in the inset of Fig.10 (a_1). For comparison, we also plot in Fig.10 (a_1) the local electron coherence $\mathcal{C}_{\mathcal{L}}$, which is negligible even though the magnetic sensitivity can be very high. Similarly, we plot in Fig.10 (a_2) the magnetic sensitivity excluding the contributions to the singlet yield production (and thereby to the magnetic sensitivity) from the local electron spin coherence and the global electron-nuclear spin coherence (as denoted by $\mathrm{D_S^{\mathbf{IC}_{\mathcal{L}}}}$ and $\mathrm{D_S^{\mathbf{GC}_{\mathcal{G}}}}$ respectively). The results show that the global electron-nuclear spin coherence is indeed indispensable to the magnetic sensitivity for the present example of flavin-superoxide radical pair. In Fig.10 $(b_1$,$b_2)$, we compare the magnetic sensitivity with/without the contributions from the local electron spin coherence and the global electron-nuclear spin coherence for a number of random hyperfine configurations. The contributions to the magnetic sensitivity by the local electron spin coherence and the global electron-nuclear spin coherence are quantified by $f^{\mathcal{LC}}(\mathrm{D_S}) = 1 - \mathrm{D_S^{\mathbf{IC}_{\mathcal{L}}}}/\mathrm{D_S}$ and $f^{\mathcal{GC}}(\mathrm{D_S}) = 1 - \mathrm{D_S^{\mathbf{IC}_{\mathcal{G}}}}/\mathrm{D_S}$ respectively (similar to the definitions in Eq.(17,18)). The results show that $f^{\mathcal{GC}}(\mathrm{D_S})$ is above 85% (and even above 90% for the high magnetic sensitivity), which clearly evidences the essential role of the global electron-nuclear spin in chemical magnetoreception. In contrast, the contribution of

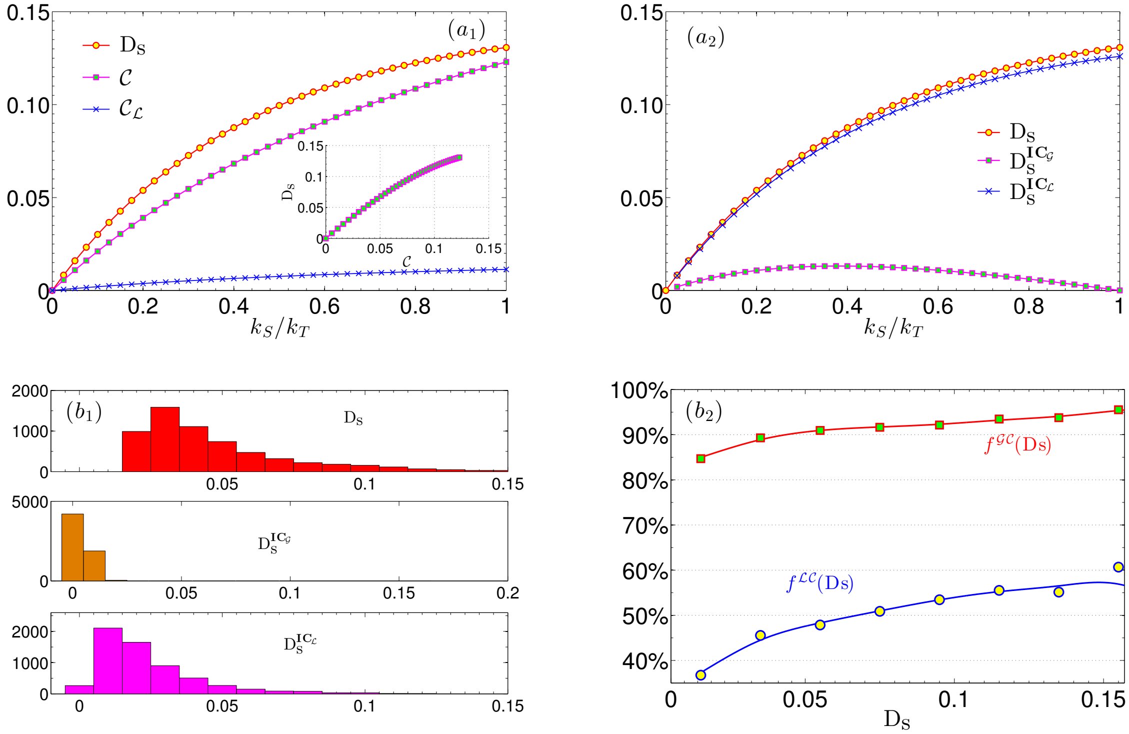

FIG. 10: $(\mathbf{a_1})$: The magnetic sensitivity $\mathrm{D_S}$, the generalized global coherence measure $\mathcal{C}$ (Eq.33) and the corresponding measure of local coherence $\mathcal{C}_{\mathcal{L}}$ (Eq.34) as a function of the ratio k_S/k_T for the flavin-superoxide radical pair. **Inset**: The magnetic sensitivity $\mathrm{D_S}$ as a function of the generalized global coherence measure $\mathcal{C}$ as defined in Eq.33). $(\mathbf{a_2})$: The magnetic sensitivity excluding the contributions from the local electron spin coherence and the global electron-nuclear spin coherence, which are quantified by $\mathrm{D_S^{\mathbf{IC}_{\mathcal{L}}}}$ and $\mathrm{D_S^{\mathbf{GC}_{\mathcal{G}}}}$ respectively, as a function of the ratio k_S/k_T for the flavin-superoxide radical pair. The common parameters for the panels of $(\mathbf{a_1})$ and $(\mathbf{a_2})$ are: the hyperfine couplings with two nitrogen nuclear spin (with spin 1) and one hydrogen nuclear spin (with spin $\frac{1}{2}$), namely N5, H5, N10, see Table I. $(\mathbf{b_1})$: The histogram of the magnetic sensitivity $\mathrm{D_S}$ **(upper)** that is larger than 0.02, and the histograms for the corresponding magnetic sensitivity $\mathrm{D_S^{\mathbf{IC}_{\mathcal{G}}}}$ **(middle)** and $\mathrm{D_S^{\mathbf{IC}_{\mathcal{L}}}}$ **(lower)** that exclude the contributions from the global electron-nuclear spin coherence and the local electron spin coherence respectively. $(\mathbf{b_2})$: The percentage of the magnetic sensitivity contributed by the local electron spin coherence and the global electron-nuclear spin coherence quantified by $f^{\mathcal{LC}}(\mathrm{D_S}) = 1 - \mathrm{D_S^{\mathbf{IC}_{\mathcal{L}}}}/\mathrm{D_S}$ and $f^{\mathcal{GC}}(\mathrm{D_S}) = 1 - \mathrm{D_S^{\mathbf{IC}_{\mathcal{G}}}}/\mathrm{D_S}$ respectively (similar to the definitions in Eq.(17,18)), averaging over the samples with $\mathrm{D_S}(\rho_0) \in [\mathrm{D_S}, \mathrm{D_S} + 0.02)$. In the panels of $(\mathbf{b_1})$ and $(\mathbf{b_2})$, the hyperfine couplings are randomly sampled with one radical coupled with three nuclei and the other radical is free of hyperfine interaction, the ratio between the singlet and the triplet reaction rate k_S/k_T is randomly chosen in the regime $[0, 1]$. The total number of random samples is 1.2×10^4. The common parameters for all the four panels are: the strength of the magnetic field is $b = 50\mu T$, and the triplet reaction rate is $k_T = 1\mu s^{-1}$, the initial system state is $\rho_0 = |\mathcal{S}\rangle\langle\mathcal{S}| \bigotimes_{k_j} \left(\mathbb{I}_{d_{k_j}}/d_{k_j}\right)$.

the local electron spin coherence (see $f^{\mathcal{LC}}(\mathrm{D_S})$ in Fig.10 (b_2)) is much less significant.

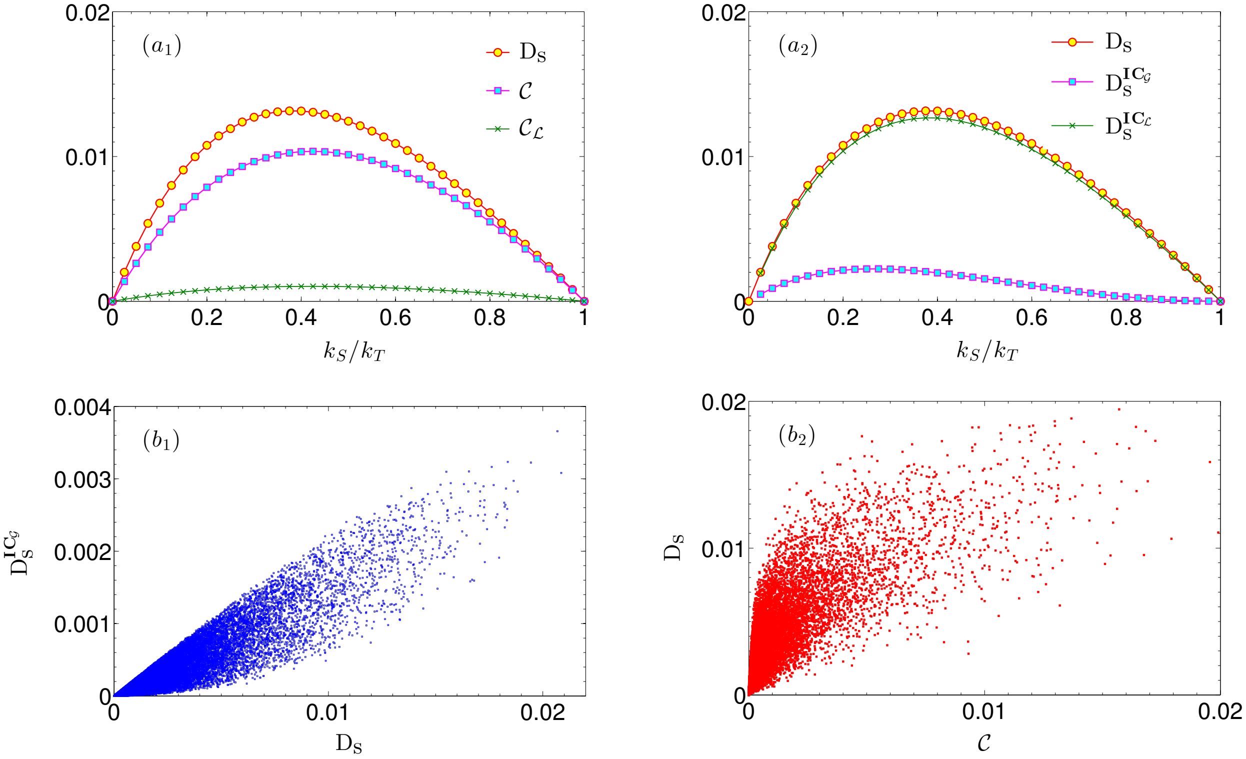

FIG. 11: $(\mathbf{a_1})$: The magnetic sensitivity $\mathrm{D_S}$, the generalized global coherence measure $\mathcal{C}$ (Eq.33) and the corresponding local coherence $\mathcal{C}_{\mathcal{L}}$ (Eq.34) as a function of the ratio k_S/k_T for the flavin-superoxide radical pair. $(\mathbf{a_2})$: The magnetic sensitivity excluding the contributions from the local electron spin coherence and the global electron-nuclear spin coherence, which are quantified by $\mathrm{D_S^{IC_{\mathcal{L}}}}$ and $\mathrm{D_S^{GC_{\mathcal{G}}}}$ respectively, as a function of the ratio k_S/k_T for the flavin-superoxide radical pair. In the panels of $(\mathbf{a_1})$ and $(\mathbf{a_2})$: the hyperfine couplings consist of two nitrogen nuclear spin (with spin 1) and one hydrogen nuclear spin (with spin $\frac{1}{2}$), namely N5, H5, N10, see Table I. $(\mathbf{b_1})$: The comparison between the magnetic sensitivity $\mathrm{D_S}$ and the corresponding one $\mathrm{D_S^{IC_{\mathcal{G}}}}$ excluding the contributions from the global electron-nuclear spin coherence. $(\mathbf{b_2})$: The magnetic sensitivity $\mathrm{D_S}$ as a function of the generalized global coherence measure $\mathcal{C}$ (Eq.33) as defined in Eq.(33). In the panels of $(\mathbf{b_1})$ and $(\mathbf{b_2})$, the hyperfine couplings are randomly sampled with one radical coupled with three nuclei and the other radical is free of hyperfine coupling, the ratio between the singlet and the triplet reaction rate k_S/k_T is randomly chosen in the regime $[0, 1]$. The total number of random samples is 2×10^4. The common parameters for all the four panels are: the strength of the magnetic field is $b = 50\mu T$, and the triplet reaction rate is $k_T = 1\mu s^{-1}$, the initial system state is chosen as the hypothetical state $\rho_0 = (\mathbb{I}_4/4) \bigotimes_{k_j} \left(\mathbb{I}_{d_{k_j}}/d_{k_j}\right)$ [S8].

In Ref.[S8], it was shown that in the case of $k_S \neq k_T$, a chemical compass starting from the hypothetical initial state $\rho_0 = (\mathbb{I}_4/4) \bigotimes_{k_j} \left(\mathbb{I}_{d_{k_j}}/d_{k_j}\right)$, which has no coherence expressed in any set of basis, can still have a certain level of magnetic anisotropy in the singlet yield. Although such an initial system state is quite unusual in realistic radical pair reactions, it is an interesting hypothetical scenario to discuss about the role of coherence in chemical magnetoreception. It is crucial to note that the imbalance of singlet and triplet reaction channels will introduce global coherence [S8], which can be captured by the proposed measure in Eq.(33) as we will show in the following. In Fig.11(a_1,a_2), we take the flavin-superoxide radical pair as an example, and vary the ratio k_S/k_T while fixing the triplet reaction rate k_T. The results demonstrate the similar essential role of the global electron-nuclear spin coherence in this scenario. In Fig.11(b_1,b_2), we calculate the magnetic sensitivity $\mathrm{D_S}$ for a number of radical pair molecules with random hyperfine configurations, in which one radical is coupled with three nuclei while the other radical pair is free of hyperfine interaction, and the ratio k_S/k_T is randomly distributed in $[0, 1]$. It can be seen that the magnetic sensitivity $\mathrm{D_S}$ is likely to be very small, nevertheless, one can still witness a direct connection between the global electron-nuclear spin coherence and the magnetic field sensitivity.

[S1] F. Cintolesi, T. Ritz, C. W. M. Kay, C. R. Timmel, P. J. Hore, *Anisotropic recombination of an immobilized photoinduced radical pair in a 50-μT magnetic field: a model avian photomagnetoreceptor*. Chem. Phys. **294**, 385 (2003).

[S2] D. J. Wineland, J. J. Bollinger, W. M. Itano, and D. J. Heinzen, *Squeezed atomic states and projection noise in spectroscopy.* Phys. Rev. A **50**, 6788 (1994).

[S3] D. Budker, and M. Romalis, *Optical magnetometry*, Nature Physics **3**, 227 - 234 (2007).

[S4] J.-M. Cai, A. Retzker, F. Jelezko, M. B. Plenio, *A large-scale quantum simulator on a diamond surface at room temperature.* Nature Physics **9**, 168 (2013).

[S5] P. London, J. Scheuer, J.-M. Cai, I. Schwarz, A. Retzker, M. B. Plenio, M. Katagiri, T. Teraji, S. Koizumi, J. Isoya, R. Fischer, L. P. McGuinness, B. Naydenov, and F. Jelezko, *Detecting and polarizing nuclear spins with nuclear double resonance on a single electron spin.* Submitted to Phys. Rev. Lett. (2013).

[S6] J.-M. Cai, G. G. Guerreschi, and H. J. Briegel, *Quantum Control and Entanglement in a Chemical Compass*, Phys. Rev. Lett. **104**, 220502 (2010).

[S7] U.E. Steiner, T. Ulrich, *Magnetic Field Effects in Chemical Kinetics and Related Phenomena*, Chem. Rev. **89**, 51 (1989).

[S8] H. J. Hogben, T. Biskup, and P. J. Hore, *Entanglement and Sources of Magnetic Anisotropy in Radical Pair-Based Avian Magnetoreceptors*, Phys. Rev. Lett. **109**, 220501 (2012).